Electronic Supplementary Material (ESI) for Journal of Materials Chemistry A.
This journal is © The Royal Society of Chemistry 2022

Supplementary data

Realizing high energy density and efficiency simultaneously in $(Bi_{0.5}Na_{0.5})_{0.7}Sr_{0.3}TiO_3$-based ceramics via introducing linear dielectric $CaTiO_3$

Xu Li[a], Jie Xing[a], Fei Wang[a], Ning Chen[a], Hao Chen[a], Qiang Chen[a], Zhi Tan[a*], Huanfu Zhou[b], Jianguo Zhu[a*]

a College of Materials Science and Engineering, Sichuan University, 610064, Chengdu, China

b College of Materials Science and Engineering, Guilin University of Technology, 541004, Guilin, China

[*] Corresponding authors.
E-mail address: tanzhi0838@scu.edu.cn (Z. Tan), nic0400@scu.edu.cn (J. Zhu).

1. Experimental procedures

1.1 Fabrications, structure, and electrical characterization of samples

(1-*x*)($Bi_{0.5}Na_{0.5}$)$_{0.7}Sr_{0.3}TiO_3$-*x*$CaTiO_3$ [*x* = 0.05, 0.10, 0.15, 0.20, 0.30, and 0.40, abbreviated as (1-*x*)BNST-*x*CT] ceramics are synthesized by conventional solid-state reaction method using the raw materials Bi_2O_3, Na_2CO_3, $SrCO_3$, TiO_2, and $CaCO_3$ (≥99% for all materials). These powders are baked at 100 °C overnight and then weighed accordingly the corresponding stoichiometry. The mixtures are ball milled in ethanol for 4 h. After drying, the mixtures are calcined at 800 °C for 4 h and then ball milled for 4 h. The achieved powders are pressed into disc samples (diameter = 8 mm, thickness = 1 mm) under uniaxial pressure of 200 MPa using PVA as binder. The disk samples are sintered at 1210-1300 °C for 2 h in air after burning out the binder at 550 °C for 4 h. To suppress the volatilization of the Bi and Na elements, the disk samples are buried in the powder of the same composition under the crucible during sintering. Furthermore, the sintered samples are polished to a thickness of 0.10 mm, and then coated by Ag electrode with a diameter of 2 mm (electrode area: 3.14 mm^2) to prevent the edge breakdown from the applied electric field, and fired at 700 °C for 30 min for further electrical measurement.

Phase structures are carried out by powder X-ray diffraction (XRD) (Cu *kα1*, 1.54059 Å, Model X'Pert PRO, PANalytical, Holland), and XRD refinements are performed via GSAS software. The microstructures are detected via field emission scanning electron microscopy (SEM) (FE-SEM, Model S4800, Hitachi, Japan). The average grain size distributions are determined by using the analytical software (Nano Measurer). The standard focused ion beam (FIB, GAIA-3 GMH FIB-SEM) sample preparation method is adopted to prepare BNST and 0.60BNST-0.40CT samples for transmission electron microscopy characterization. The selected area electron diffraction (SAED) and high-resolution transmission electron microscopy (HR-TEM) patterns are performed by the JEOL JEM-300F. Dielectric responses are evaluated with a precision impedance analyzer (4294A, Hewlett-Packard Co, Palo Alto, CA). Polarization electric field (*P*-*E*) loops are characterized using the ferroelectric test system (RT66, Radiant Technologies, NM,

USA). To check the domain structure, a piezoresponse force microscope (PFM, MFP-3D, USA) is applied by Pt/Ir-coated conductive tips (Nanosensors, Neuchatel, Switzerland) with an AC tip voltage of 3 V and out-of-plane mode. The discharge performances are characterized using a dielectric charge and discharge test system (PK-CPR1701, PolyK Technologies, PA, USA).

2. Results and Discussion

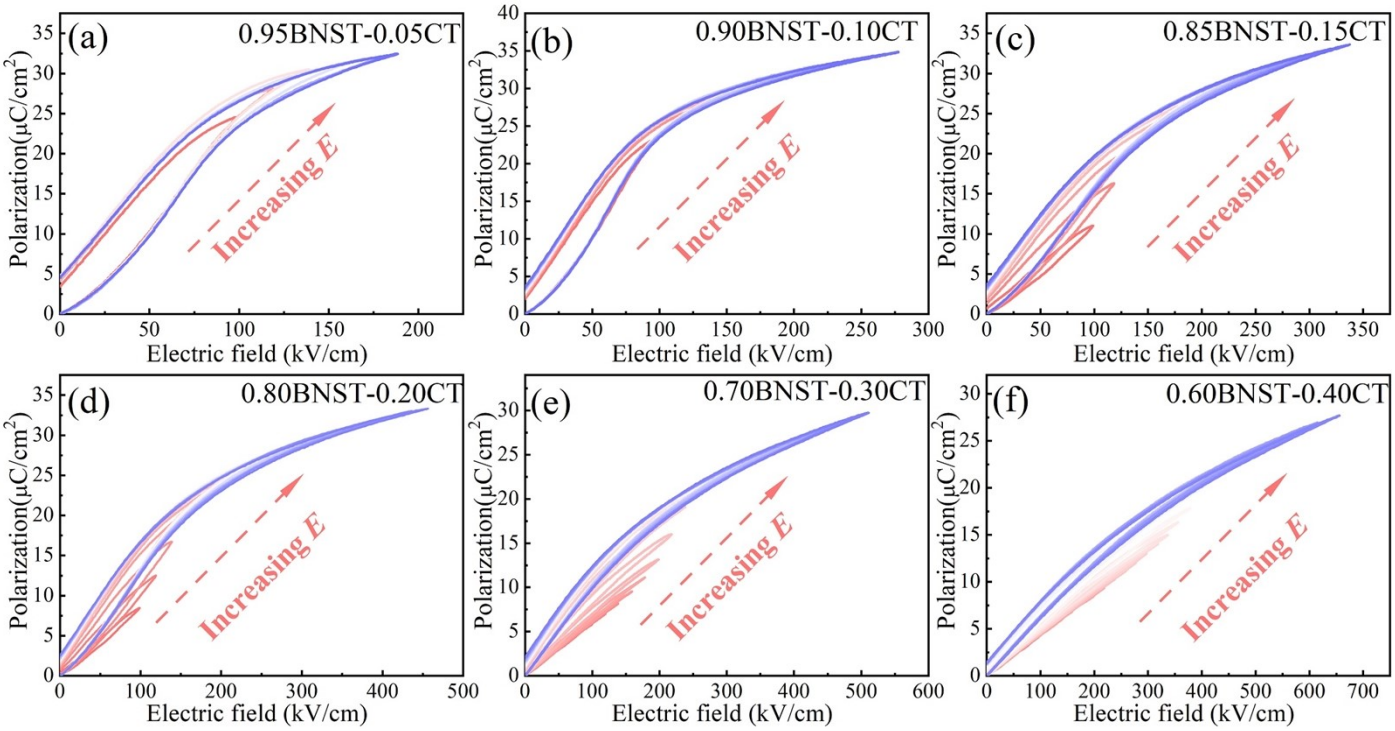

Fig. S1 (a)-(f) Unipolar *P*-*E* loops of (1-*x*)BNST-*x*CT ceramics under various electric fields.

For ferroelectric with large size domain (low CT content), their polarization increases rapidly and saturates at a low external electric field induction [**Fig.S1(a)**, **Fig.S1(b)**, and **Fig.S7(a)**]. Unlike ferroelectric with low CT content, the presence of weak polar phases (or absence of polar phases) in ceramics with high CT content [**Fig. 3(f_1)**] means that they need to induce polar phases at a higher electric field. In other words, a linear-like *P*-*E* loop is observed under low electric field [**Figs.S1(c)-(f)**]. Similar phenomena have been reported in many systems with high CT content.

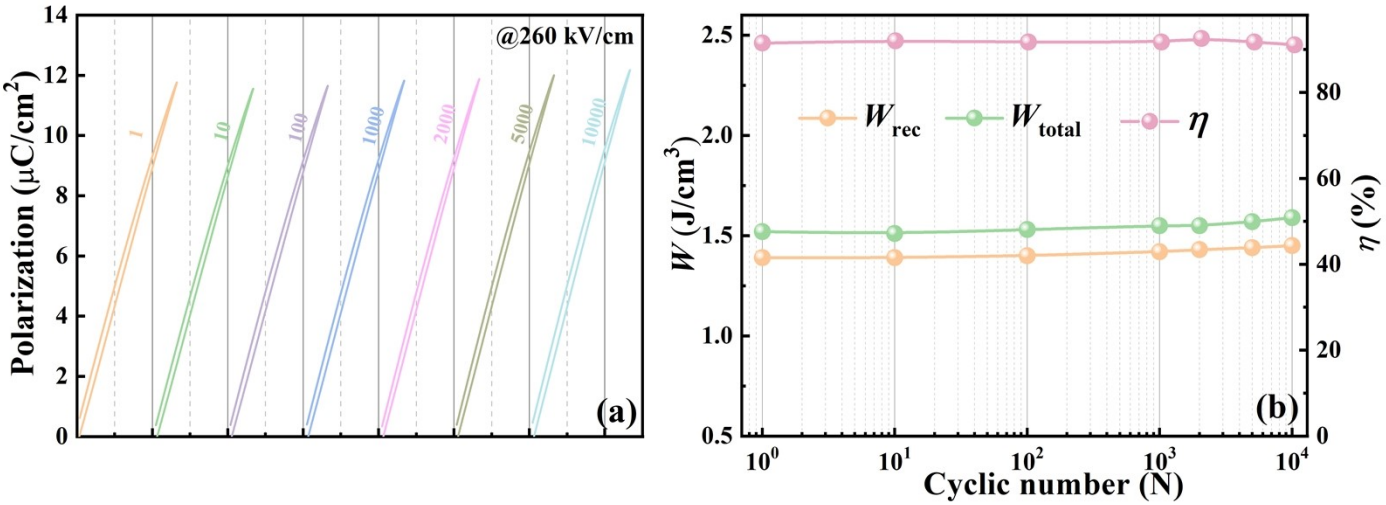

Fig. S2 Fatigue performances of the 0.60BNST-0.40CT ceramics.

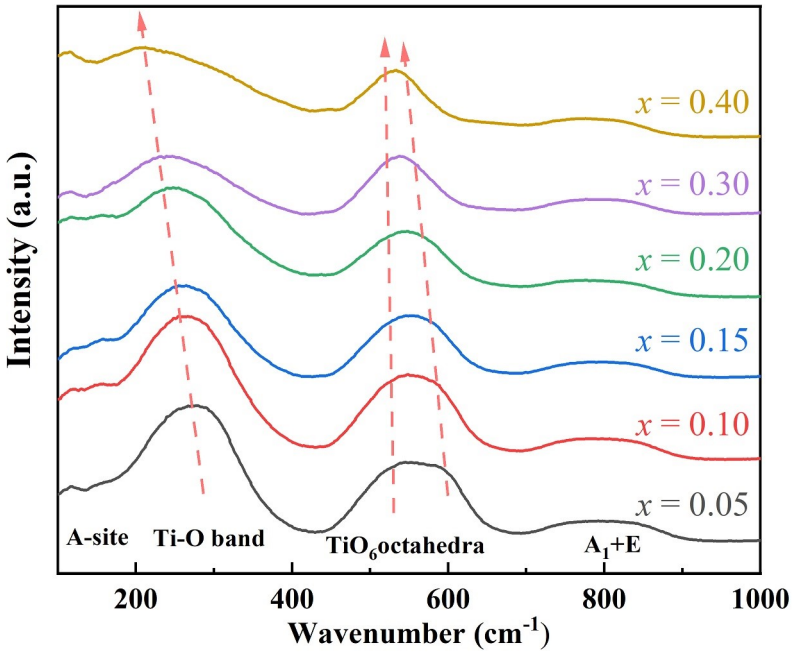

Fig. S3 Raman spectra of the (1-*x*)BNST-*x*CT ceramics under the room temperature.

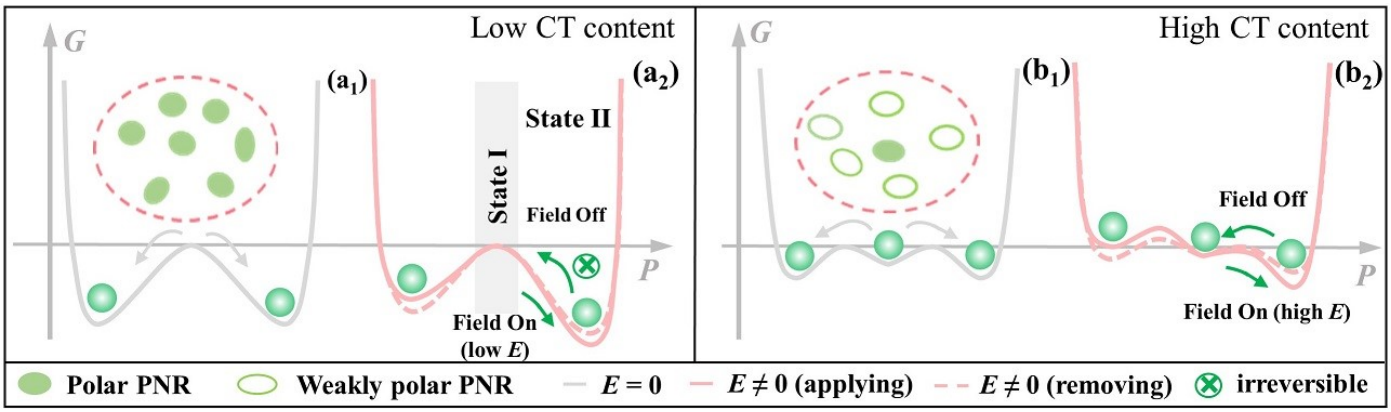

Fig. S4 Before and after applying the electric field, schematic free energy curves and the corresponding schematic domain structures with increasing CT content.

Since HR-TEM, VPFM and Raman analyses only reflect the local phenomenon, herein a schematic model is used to quantitatively illustrate high η and delayed saturation polarization in (1-x)BNST-xCT system with the support of Landau-Devonshire theory. The free energy (G) with various states versus polarization (P) expansion can be described as follows [1, 2]:

$$G = \alpha P^2 + \beta P^4 + \delta P^6, \quad (1)$$

$$G = \alpha P^2 + \beta P^4 + \delta P^6 - EP, \quad (2)$$

where α, β, δ are the expansion coefficients. Based on the equation (2), the polarization is reoriented after applying the external electric field, and the free energy curve is dragged down to the low right [the solid lines in **Figs. S4(a_2)** and **(b_2)**]. After removing the external fields, the curve will partly rebound because of the existence of local random fields [the dashed lines in **Figs. S4(a_2)** and **(b_2)**]. For ferroelectric (FE) with large size domain (low CT content), their polarization rises rapidly and saturates under the low external electric field [**Fig. 2(a)**]. And it is hard to cross the energy barrier after removing the electric field due to the high intrinsic energy barrier in FE [the lines in **Figs. S4(a_2)**], thus resulting in low η. Unlike conventional FE, the presence of weak polar phases (or absence of polar phases) in ceramics with high CT content [**Fig. 3(f_1)**] means that they need to induce polar phases at a higher electric field. The long-range polar phase (State II) induced via the field will go back the weakly coupled polar state (State I) due to the low energy potential of relaxor ferroelectrics [3], resulting in a macroscopic relaxor state with high η. These behaviors further explain the origin of the delayed polarization saturation and large η in high CT content.

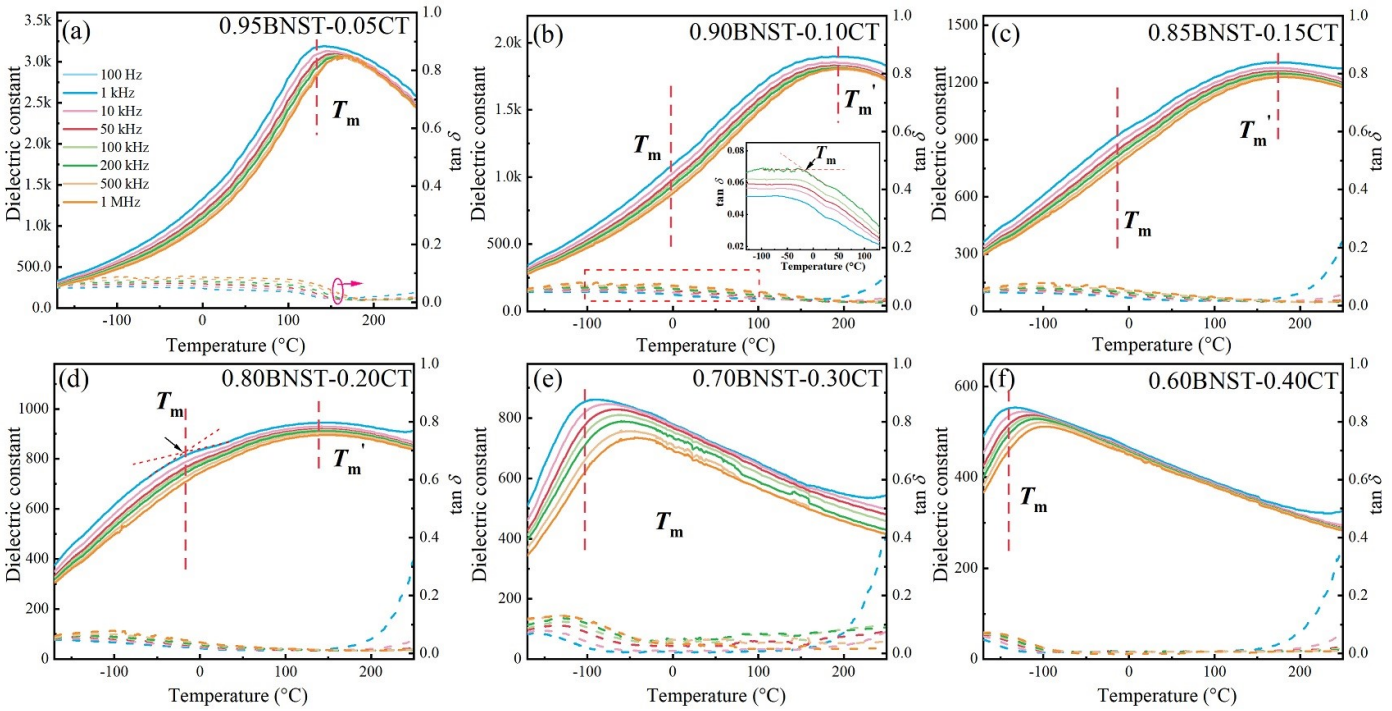

Fig. S5 Temperature dependence of ε_r and tan δ of (1-x)BNST-xCT ceramics under various frequencies.

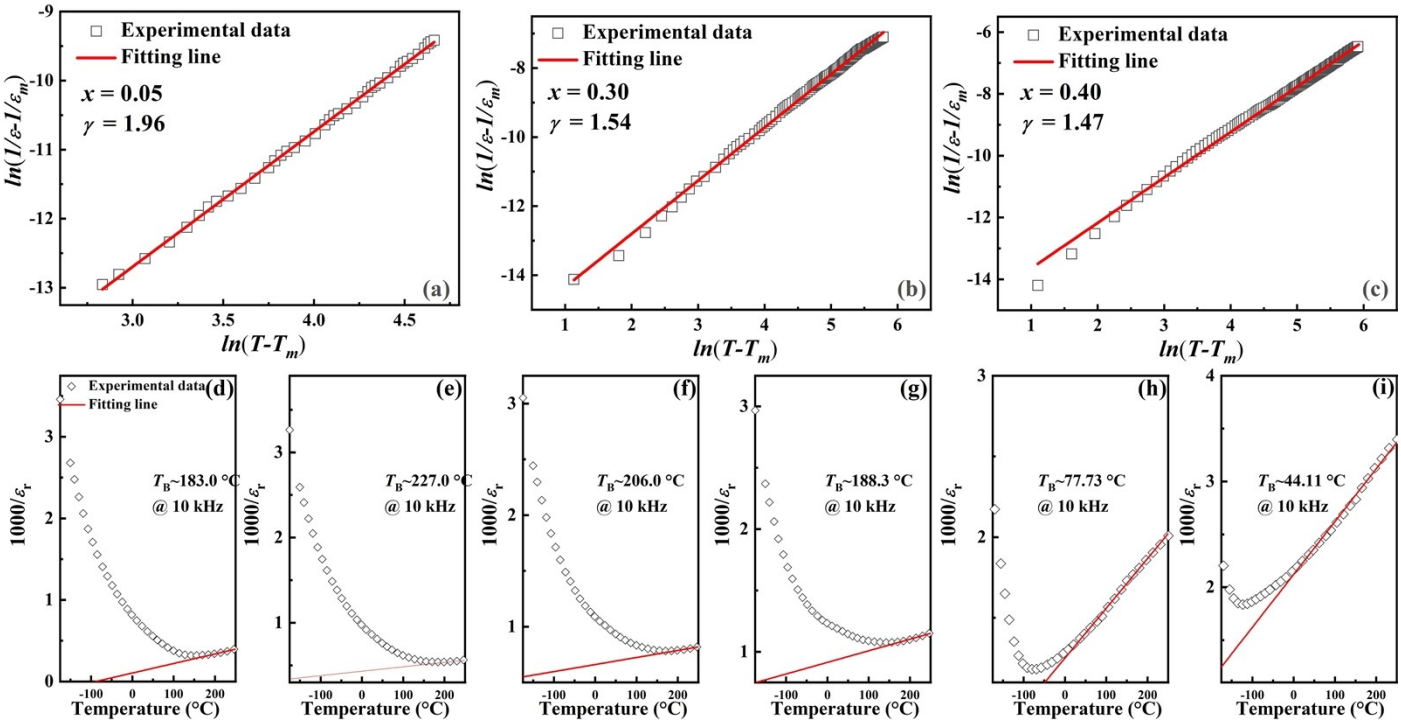

Fig. S6 (a)-(c) Plots of $\ln(1/\varepsilon_r-1/\varepsilon_m)$ versus $\ln(T-T_m)$ of (1-x)BNST-xCT (x = 0.05, 0.30, and 0.40) ceramics at 10 kHz. (d)-(i) Temperature dependence of reciprocal of dielectric ε_r in (1-x)BNST-xCT ceramics.

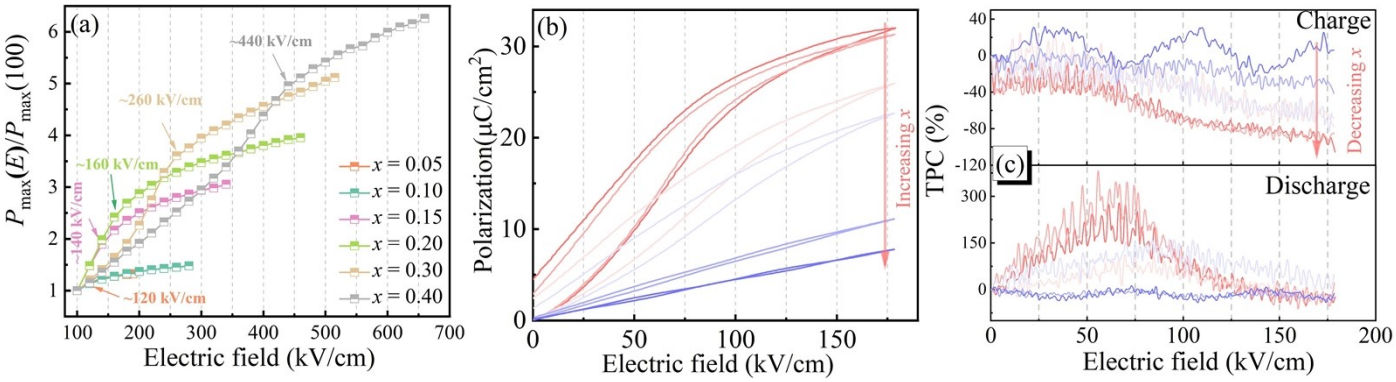

Fig. S7 (a) Unipolar *P*-*E* hysteresis loops at 180 kV/cm for the (1-*x*)BNST-*x*CT ceramics. (b) Variation of TPC with external electric fields during charging and discharging. (c) The P_{max} values are normalized to the P_{max} values at 100 kV/cm for the (1-*x*)BNST-*x*CT ceramics.

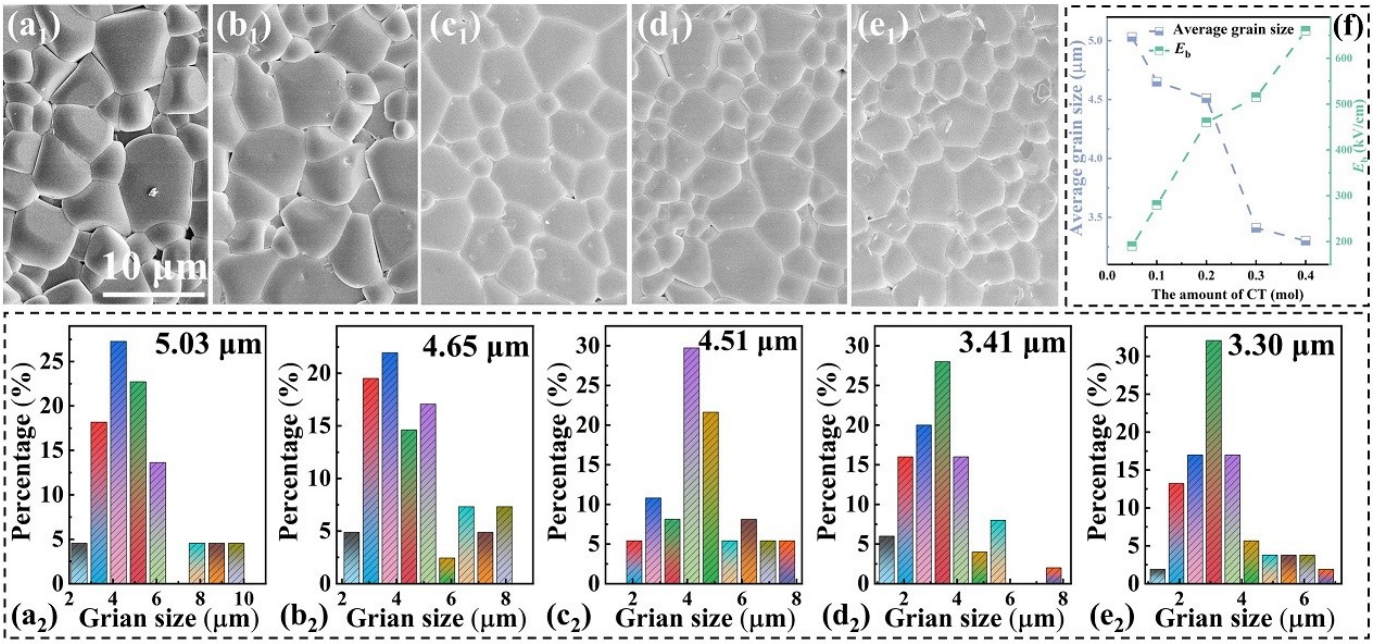

Fig. S8 (a_1)-(e_1) SEM and (a_2)-(e_2) corresponding average grain size distribution of (1-*x*)BNST-*x*CT ceramics in selected areas. (f) The average grain size and E_b as a function of CT content.

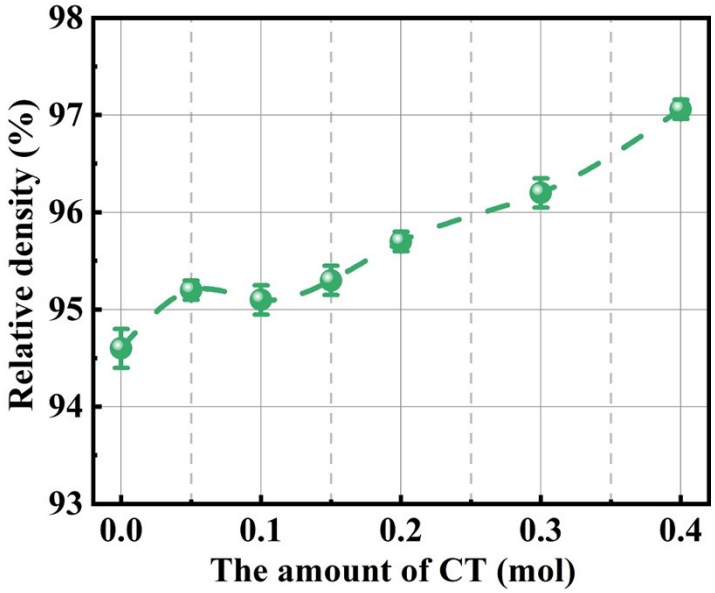

Fig. S9 Relative densities of the (1-*x*)BNST-*x*CT ceramics.

The relative densities of all as-prepared samples are provided, as shown in **Fig. S9**. All ceramics exhibited high relative density (> 94.0%), which is consistent with dense microstructures [**Figs. S8(a_1)-(e_1)**]. With increasing CT content, the relative densities of the ceramics show a slightly increase, which is conducive to further optimizing E_b.

Table S1 Summary of the Vogel-Fulcher fitting parameters of (1-*x*)BNST-*x*CT ceramics.

Component	f_0 (Hz)	T_f (K)	E_a (eV)
0.05	2.07E11	398.26	0.041
0.10	5.00E10	210.77	0.045
0.15	5.00E10	198.35	0.048
0.20	5.00E10	181.51	0.080
0.30	5.00E12	141.54	0.108
0.40	5.00E11	71.19	0.120

Table S2 The ε_r of the grains and grain boundaries of (1-*x*)BNST-*x*CT (*x*=0.05, 0.30, and 0.40) ceramics.

Component	$\varepsilon_g(0)$	$\varepsilon_{gb}(0)$
0.05	1544.80	154.48
0.30	772.70	77.27
0.40	459.50	45.95

References

[1] C. Ahn, C. Hong, B. Choi, H. Kim, H. Han, Y. Wang, W. Jo, K. Wang, J. Li, J. Lee, I. W. Kim, J. Korean. Phys. Soc., 2016, **68**, 1481-1494.

[2] V. Shvartsman, D. Lupascu, D. Green, J. Am. Ceram. Soc., 2012, **95**, 1-26.

[3] N. Liu, R. Liang, Z. Zhou, X. Dong, J. Mater. Chem. C., 2018, **6**, 10211-10217.